j Med Imaging(ScholarGen) Volume 4(2021) 01, pp 33-41 ISSN : 2635-4608

DOI http://dx.doi.org/10.31916/sjmi2021-01-04

Evaluation of Brain Glioblastoma Images Using Podoplanin-targeted Manganese Ferrite in 9.4T MRI

Seung-Hyun Yang,[1] Yong-Min Huh,[2,*] Hwunjae Lee[1,2,3*]

,Received : 5 July 2021 / Accepted : 2 November 2021 / Published online 28 December 2021

ⓒThe Author(s) 2021

Abstract To detect brain glioblastoma, which is difficult to treat and has a very poor prognosis, a method for early detection on magnetic resonance imaging (MRI) using podoplanin (PDPN), a biomarker for glioblastoma, is proposed in the present study. Magnetic nanoparticle (MNP)-PDPN was prepared using manganese (Mn) iron targeting PDPN. Axial and coronal images of 3 brain model (GSC11_G19_No.4) mice were acquired with a 9.4T high-magnetic field MRI, and an experiment was conducted. The mean value and standard deviation were larger in the image after the contrast agent (MNP-PDPN) was injected, confirming that injection of the contrast agent improved the image of the brain glioblastoma area. In addition, the area of the segmented image using the region of interest was large in the image obtained after injection of contrast agent (MNP-PDPN). PSNR evaluation showed values from 13.77 dB–20.09 dB. In conclusion, in the present study, the MNP-PDPN contrast agent was shown useful for early detection of brain glioblastoma. Future research is needed to develop a theragnostic technology to diagnose and treat glioblastoma simultaneously using MNP-PDPN.

Seung-Hyun Yang,[1] Yong-Min Huh,[2]
Hwunjae Lee[1,2,3*] Corresponding author(✉)

[1] Department of Radiology, College of Medicine, Yonsei University, Seoul 03722, Republic of Korea

[2]YUHS-KRIBB Medical Convergence Research Institute, Yonsei University Health System, Seoul 03722, Republic of Korea

[3]Graduate Program of Nanoscience and Technology, College of Medicine, Yonsei University, Seoul 03722, Republic of Korea

Key words: Glioblastoma, Early detection, Contrast agent, MRI evaluation, PSNR

I. Introduction

Modern medicine is based on understanding human health and controlling the course of chronic diseases, correcting disabling physical conditions, and treating molecular deficiencies [1]. The expected medicine of the future will detect diseases at an early stage and develop into personalized and precision medicine based on individual diseases [2]. A brain tumor is a mass of cells that grow abnormally, and various types exist. Brain tumors can be benign or malignant, as well as primary or metastatic . Growth speed of a brain tumor varies greatly depending on the type of brain tumor, and the location and growth rate of the brain tumor have a significant effect on the nervous system. Among brain tumors, glioblastoma multiforme is a deadly intracranial cancer with an aggressive malignant progression. This tumor is highly resistant to conventional combination therapies such as traditional radiation and chemotherapeutic agents [3]. Therefore, early detection of glioblastoma is very important for effective treatment. Traditionally, magnetic

resonance imaging (MRI) plays an important role in the imaging of angiogenesis in the tumor microenvironment and is important for predicting cancer metastasis [4]. However, MRI has low sensitivity. The use of optical imaging can increase sensitivity and compensate for the MRI shortcomings [5]. In particular, optical imaging can increase the contrast and sensitivity to new blood vessels, creating a synergistic effect. In the present manuscript, a technique is proposed for early detection of glioblastoma on MRI using podoplanin (PDPN) as a biomarker to detect glioblastoma, which is difficult to treat and has a very poor prognosis. Therefore, magnetic nanoparticle (MNP)-PDPN contrast agent was developed using manganese (Mn) iron targeting PDPN. For the experiment, images of 9 mouse brains (GSC11_G19_No.4) were acquired with a 9.4T high-magnetic field MRI device. The image processing results confirmed good resolution using the MNP-PDPN contrast agent. Future research goals include synthesizing the therapeutic agent in MNP-PDPN contrast agent to develop theragnostic technology targeting glioblastoma cells.

Ⅱ. Materials and methods

1. Animal model and experimental procedure

All animal experiments were conducted with the approval of the Association for Assessment and Accreditation of Laboratory Animal Care International. Female BALB/C-Slc nude mice 7–8 weeks of age were anesthetized by intraperitoneal injection of Zoletil/Rompun mixture, and 200 mL of saline containing 1.0 × 107 GSC11 cells was injected into the brain. After cancer cell implantation, MRI was performed at 2–3 weeks. Glioblastoma multiforme is a lethal intracranial cancer that exhibits an aggressive malignant progression highly resistant to conventional combination therapies such as radiation and chemotherapy agents [3]. Therefore, early detection of glioblastoma is critical for effective treatment. Traditionally, because MRI plays a major role in the imaging of neovascularization in the tumor microenvironment, predicting the metastasis of cancer is very important [4]. However, MRI has low sensitivity, and use of optical imaging enables an increase in sensitivity and compensates for the disadvantages of MRI [5]. In particular, optical imaging can increase the contrast and sensitivity for new blood vessels, which can result in great synergy.

2. *Glioblastoma biomarkers*

Podoplanin (PDPN) is a transmembrane mucin-like protein broadly associated with lymphatic endothelium and lymphangiogenesis, and it augments the separation of blood and lymphatic vessels during embryonic development. Widespread PDPN expression has been described in various human tumors in which platelet aggregation caused by PDPN through C-type lectin-like receptor-2 (CLEC-2) has been associated with metastasis [6]. In addition, PDPN has been linked to cytoskeleton regulation and increased migration and invasion. In gliomas, a grade-dependent expression of PDPN usually is found in tumor cells.

3. *Magnetic nanoparticles*

Manganese ferrite has become an important research area in the past two decades mainly due to its magneto-optical and magneto-resistive properties, which are applied in various fields from technology to medicine [7, 8]. Ferrites are usually metal oxides with iron as the main metallic constituent. These ferrites have a superparamagnetic property that

allows wide use in the field of biomedical applications [9]. However, as most are susceptible to weak chemical stability, surface modification or doping of other elements is necessary. Therefore, researchers use doping elements such as Co, Mg, Mn, Zn, and Ni to produce chemically stable ferrites in biological systems and for tuning their magnetic behavior [10]. Among ferrites, Mn ferrite is a well-known soft magnetic material with high coercivity, moderate magnetization, excellent physiochemical stability, and high cubic magneto-crystalline anisotropy, for which it is used for various biological applications [11]. Mn-doped ferrite is an efficient MRI contrast agent compared with magnetite because it has the same saturation magnetization as iron oxide but possesses a higher order of crystalline anisotropy, causing slower magnetic moment relaxation [12]. Furthermore, anisotropic nanostructures have attracted much interest in recent years [13]. Therefore, various synthesis techniques have been developed to produce different nanostructure shapes such as rods, prisms, octahedrals, and cubes.

4. Image acquisition

All MRI experiments were performed using a 9.4T Bruker BioSpec scanner (RF SUC 400 1H M-BR-LIN ROAD, Bruker Medical Systems, Germany).

Table 1. Results of 9.4T MRI

	Agent Inj.	*T2 Axial Image*	*T2 Coronal Image*
Model_1	*Before inj.*	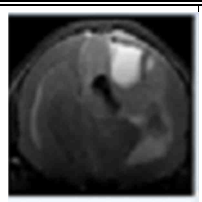	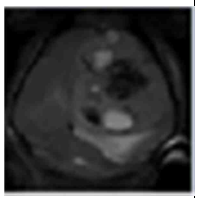
Model_2	*After inj.*	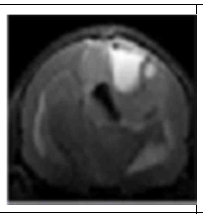	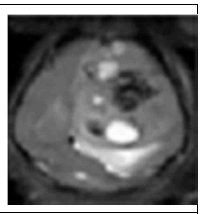
	Before inj.	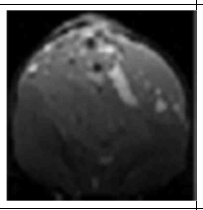	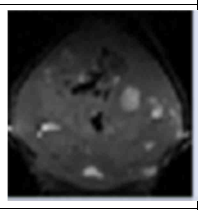
	After inj	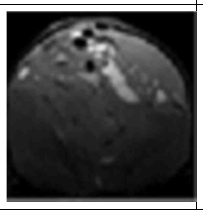	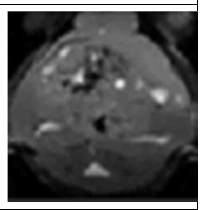
Model_3	*Before inj*	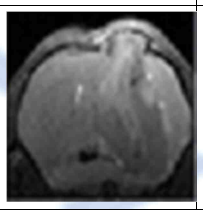	
	After inj.	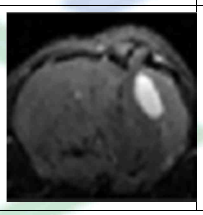	

5. Image quality evaluation based on contrast agent injection

Image quality evaluation characterizes the content and texture of an image. Basically, evaluation metrics can be categorized into primary, secondary, and higher-order scales. Primary metrics focus on properties such as mean intensity, standard deviation, and variance. Therefore, first-order metrics only measure individual pixels in the image and do not account for spatial relationships between pixels, ignoring neighbor relationships. Conversely, quadratic or higher metrics measure the properties of two or more pixels relative to each other at a specific location. In medical images, the mean often is used

as a matrix representative value of pixels. The standard deviation of one of the scatter plots is representative of dispersion of the medical image pixel data around the mean. A standard deviation close to 0 indicates that the data values are concentrated near the mean, and a larger standard deviation indicates the data values are spread more widely. Peak signal-to-noise ratio (PSNR) is the maximum signal-to-noise rati, an objective measurement method that numerically indicates the difference between the image before contrast agent injection and the image after contrast agent injection during medical image evaluation. PSNR is most easily defined as the mean square error (MSE). Given a before contrast agent injection image m × n monochrome image I and an after contrast agent injection image approximation K, MSE is defined as:

$$MSE = \frac{1}{m\,n}\sum_{i=0}^{m-1}\sum_{j=0}^{n-1}[I(i,j) - K(i,j)]^2 \quad \text{---------(1)}$$

The PSNR (in dB) is defined as:

$$\begin{aligned} PSNR &= 10 \cdot \log_{10}\left(\frac{MAX_I^2}{MSE}\right) \\ &= 20 \cdot \log_{10}\left(\frac{MAX_I}{\sqrt{MSE}}\right) \\ &= 20 \cdot \log_{10}(MAX_I) - 10 \cdot \log_{10}(MSE) \end{aligned} \quad \text{-----(2)}$$

Here, MAX_I is the maximum possible pixel value of the image. When the pixels are represented using 8 bits per sample, MAX_I is 255. More generally, when samples are represented using linear pulse-code modulation (PCM) with B bits per sample, MAX_I is 2^B-1. Image processing for image evaluation was performed with an M-program using MATLAB image processing toolbox as shown in Figure 1.

```
ROI_segmentation.m  Untitled*  +
    thresholdValue = 127;
    binaryImage = originalImage > thresholdValue; % Bright objects will be chosen if you use >.
    % ========== IMPORTANT OPTION ============================================================
    % Use < if you want to find dark objects instead of bright objects.
    %   binaryImage = originalImage < thresholdValue; % Dark objects will be chosen if you use <.
    % Do a "hole fill" to get rid of any background pixels or "holes" inside the blobs.
    binaryImage = imfill(binaryImage, 'holes');
    % Show the threshold as a vertical red bar on the histogram.
    hold on;
    maxYValue = ylim;
    line([thresholdValue, thresholdValue], maxYValue, 'Color', 'r');
    % Place a text label on the bar chart showing the threshold.
    annotationText = sprintf('Thresholded at %d gray levels', thresholdValue);
    % For text(), the x and y need to be of the data class "double" so let's cast both to double.
    text(double(thresholdValue + 5), double(0.5 * maxYValue(2)), annotationText, 'FontSize', 10, 'Color', [0 .5 0]);
    text(double(thresholdValue - 70), double(0.94 * maxYValue(2)), 'Background', 'FontSize', 10, 'Color', [0 0 .5]);
    text(double(thresholdValue + 50), double(0.94 * maxYValue(2)), 'Foreground', 'FontSize', 10, 'Color', [0 0 .5]);
    % Display the binary image.
    subplot(3, 3, 3);
    imshow(binaryImage);
    title('Binary Image, obtained by thresholding', 'FontSize', captionFontSize);
```

Figure 1. MATLAB program for the experiment

III. Experiment and Results

1. *Experimental process*

All MRI experiments were performed using a 9.4T Bruker BioSpec scanner (RF SUC 400 1H M-BR-LIN ROAD, Bruker Medical Systems). The following parameters were used at room temperature for T2 and FLASH sequences: T2 sequence (Echo = 1, TR = 2300 ms, TE = 22.0 ms, FA = 180 deg, TA = O h 4 m 54 s 400 ms, NEX = 2, FOV = 4.00); FLASH sequence (TR: 280.0 ms , FA = 25 deg, TA = O h 7 m 10 s, NEX = 4, FOV = 4.00). The experiment was evaluated by comparing the images before and after injection of contrast agent in the order shown in Figure 2.

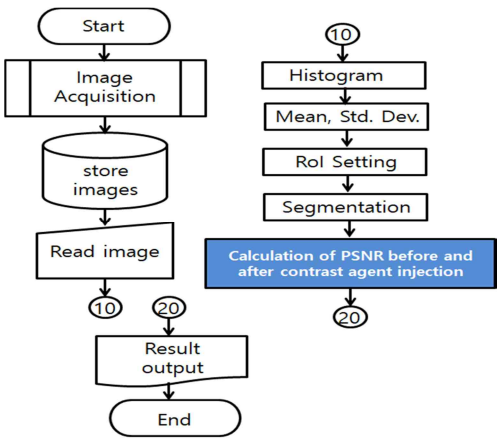

Figure 2. Experiment flow chart

2. *Experimental results*

To evaluate the 9.4T MRI images of brain glioblastoma before and after contrast agent injection, the acquired images were pre-processed with 256 × 256-pixel 256-level grayscale images. The mean value and standard deviation of each pixel of the pre-processed original image were calculated. Then, the distribution of pixels was confirmed on a histogram of the image, and the image was segmented after setting the region of interest. Tables 2–7 show the experimental results of T2 axial and T2 coronal images before and after contrast agent injection in experimental Models 1–3.

Table 2. T2_Axial experimental results of Model_1

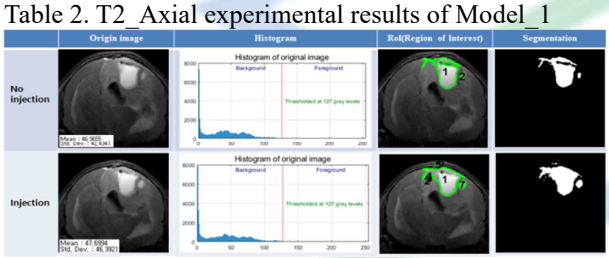

Table 3. T2_Coronal experimental results of Model_1

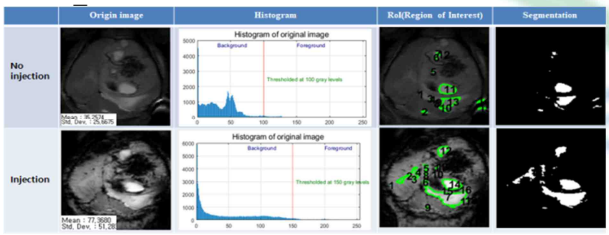

Table 4. T2_Axial experimental results of Model_2

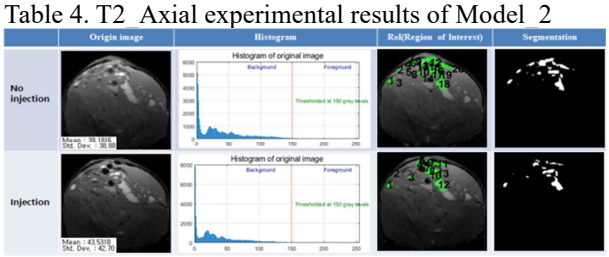

Table 5. T2_Coronal experimental results of Model_2

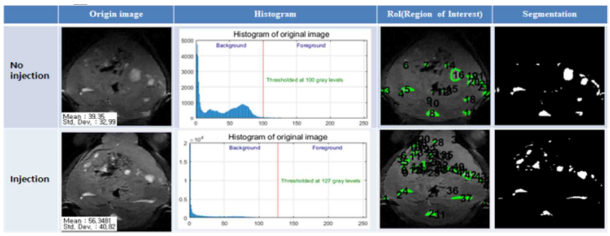

Table 6. T2_Axial experimental results of Model_3

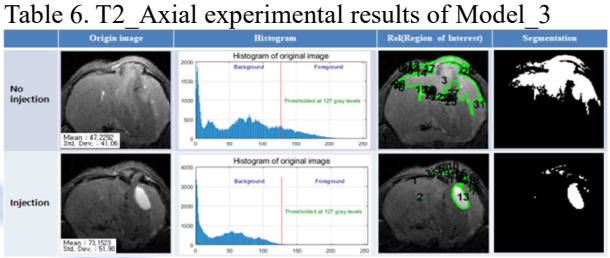

Table 7. T2_Coronal experimental results of Model_3

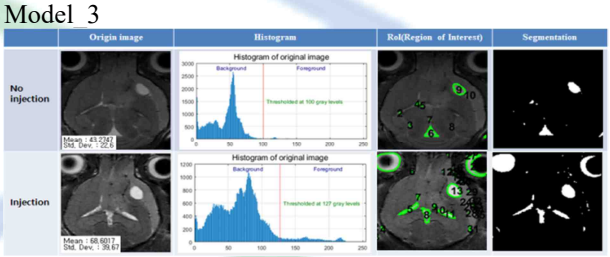

The experimental results showed larger mean and standard deviation in the image after contrast agent injection than in the image before injection. In the histogram, the background showed a much larger distribution of pixels, and the foreground area (with glioblastoma) showed a small value. When the image was segmented with the region of interest as the boundary of the threshold value, the image after contrast agent injection showed a larger segmented region than did the image before injection.

Table 8 shows the MSE and PSNR calculations for T2 sequence axial images before and after contrast agent injection for experimental Model 1. In the experiment, MSE was 636, root mean square error (RMSE) was 25.22, and PSNR was 20.09 dB.

Table 8. T2 axial images of experimental Model 1

Pre-injection	*Post-injection*	*Result*	
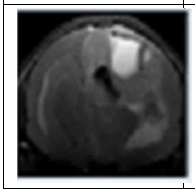	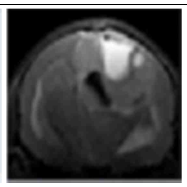	MSE	636.2
		RMSE	25.22
		PSNR	20.09

Table 9 shows the MSE and PSNR calculations for T2 sequence coronal images before and after contrast agent injection in experimental Model 1. In the experiment, MSE was 2,727, RMSE was 52.22, and PSNR was 13.77 dB.

Table 9. T2 coronal images of experimental Model 1

Pre-injection	*Post-injection*	*Result*	
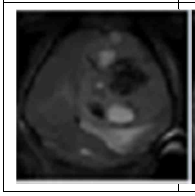	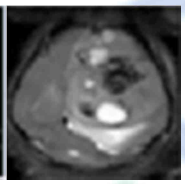	MSE	2,727
		RMSE	52.22
		PSNR	13.77

Table 10 shows the MSE and PSNR calculations for T2 sequence axial images before and after contrast agent injection in experimental Model 2. In the experiment, MSE was 699.90, RMSE was 26.46, and PSNR was 19.68 dB.

Table 10. T2 axial images of experimental Model 2

Pre-injection	*Post-injection*	*Result*	
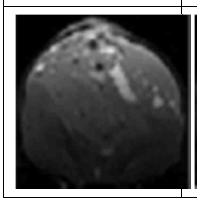	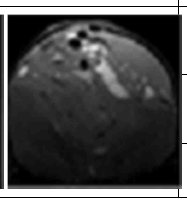	MSE	699.89
		RMSE	26.455
		PSNR	19.680

Table 11 shows the MSE and PSNR calculations for T2 sequence coronal images before and after contrast agent injection in experimental Model 2. In the experiment, MSE was 1,570, RMSE was 39.62, and PSNR was 16.70 dB.

Table 11. T2 coronal images of experimental Model 2

Pre-injection	*Post-injection*	*Result*	
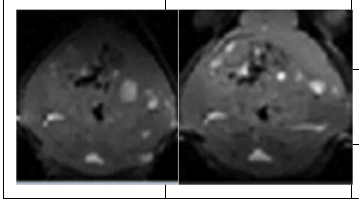		MSE	1,570.33
		RMSE	39.6274
		PSNR	16.1709

Table 12 shows the MSE and PSNR calculations for T2 sequence axial images before and after contrast agent injection in experimental Model 3. In the experiment, MSE was 2,006, RMSE was 44.78, and PSNR was 15.11 dB.

Table 12. T2 axial images of experimental Model 3

Pre-injection	*Post-injection*	*Result*	
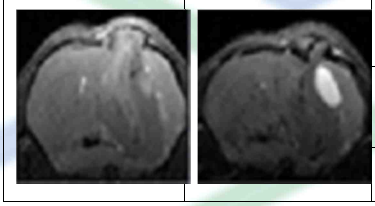		MSE	2,005.9
		RMSE	44.78
		PSNR	15.10

Table 13 shows the MSE and PSNR calculations for T2 sequence coronal images before and after contrast agent injection in experimental Model 3. In the experiment, MSE was 1,983, RMSE was 44.53, and PSNR was 15.16 dB.

Table 13. T2 coronal images of experimental Model 3

Pre-injection	*Post-injection*	*Result*	
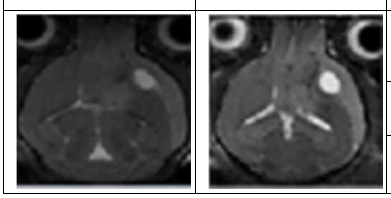		MSE	1,983
		RMSE	44.53
		PSNR	15.15

IV. Discussion

Improving medical imaging or visual quality of digital images can be subjective, and it is uncertain whether one method produces a better-quality image. Therefore, establishing quantitative/empirical measures to compare the effect of image enhancement on image quality is necessary [14]. Quality analysis of medical images characterizes the content and texture of the image. Basically, rating scales can be classified into primary (first-order), secondary (second-order), and higher-order scales. Primary metrics focus on properties such as mean intensity, standard deviation, and variance and only measure individual pixels in the image. A first-order metric does not account for spatial relationships between pixels, leaving out neighbor relationships. A quadratic or higher metric measures the properties of two or more pixels relative to each other at a specific location. MSE is used to measure the difference between an expected outcome and the actual outcome. This metric is a variance measure and can be used to analyze image enhancements such as noise and blur removal [14]. The PSNR is an important metric used to measure the quality of the image when enhanced by a contrast agent. Higher PSNR value indicates higher quality rate. The MSE determines the PSNR value. When comparing two images, PSNR is calculated as the MSE between the pixel intensities and taking the ratio of the maximum possible intensity to the result of the calculation. The standard value of PSNR is 35–40 dB. In general, a higher PSNR value corresponds to a better-quality image. The PSNR standard value is subjected to correlation analysis and depends on MSE, which is indirectly proportional to the PSNR. The histogram represents the frequency of differences in intensity between two images [14].

1. Mean and standard deviation before and after contrast agent injection

Average intensity plays a role in image contrast; the higher is the value, the greater is the contrast in the image. The average value represents the contribution of individual pixel intensities to the overall image. The standard deviation quantifies the amount of change in the image. This is an optimal metric for evaluating the quality of enhanced images and can be used in applications where images are enhanced by injecting a contrast agent. Table 8 shows the pixel mean values and standard deviations of the axial and coronal plane images before and after injection of contrast agent in experimental Models 1–3; the mean value and the standard deviation are larger in the image after contrast agent injection.

Table 14. Mean and standard deviation

Experimental Model	Contrast agent Injection	Axial		Coronal	
		Mean	Std. Dev.	Mean	Std. Dev.
1	No Injection	46.96	42.43	35.25	25.67
	Injection	47.7	46.39	77.37	51.28
2	No Injection	39.18	38.88	39.35	32.99
	Injection	43.53	42.7	56.35	40.82
3	No Injection	47.23	41.06	43.27	22.6
	Injection	73.15	51.9	68.6	39.67

Figures 3 and 4 are graphs showing the contents of Table 14; the images after injection of the contrast agent in experimental Models 1–3 show larger values.

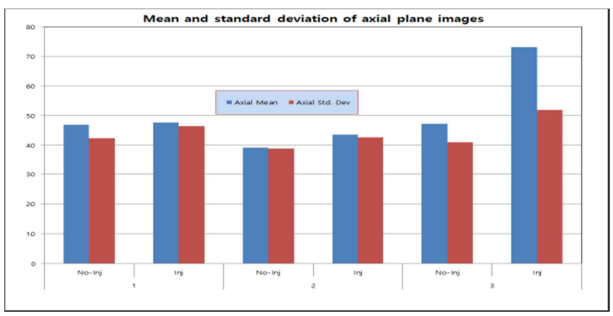

Figure 3. Mean and standard deviation of axial plane images

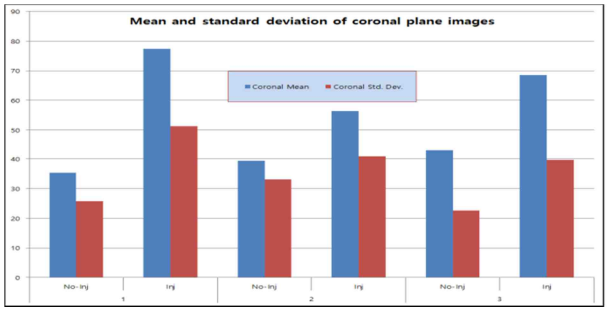

Figure 4. Mean and standard deviation of coronal plane images

2. PSNR evaluation before and after contrast agent injection

Higher PSNR value indicates higher quality rate. The MSE determines the PSNR value. When comparing two images, PSNR is calculated using the MSE between the pixel intensities and the ratio of the maximum possible intensity to the result of the calculation. In general, a higher PSNR value corresponds to a higher-quality image. The PSNR standard value is subjected to correlation analysis and depends on MSE, which is indirectly proportional to the PSNR.

Table 15. MSE, RMSE, and PSNR values

Model	Plane	MSE	RMSE	PSNR (dB)
Model_1	Axial	636.25	25.22	20.09
	Coronal	2,727	52.22	13.77
Model_2	Axial	699.9	26.46	19.68
	Coronal	1,570	39.63	16.17
Model_3	Axial	2,005	44.79	15.11
	Coronal	1,983	44.53	15.16

V. Conclusion

Herein, a method was proposed for early detection of glioblastoma based on MRI using PDPN as a biomarker to detect glioblastoma, which is difficult to treat and has a very poor prognosis. The mean value, standard deviation, histogram, image segmentation, and PSNR of images acquired before and after contrast agent injection using the 9.4T MRI device were evaluated. Consequently, the following conclusions were obtained.

1. The mean value and standard deviation showed larger values in the image after contrast agent (MNP-PDPN) was injected, confirming that injection of the contrast agent enhanced the image of the brain glioblastoma area.

2. The area of the segmented image using the region of interest was large in the image obtained after injection of the contrast agent (MNP-PDPN), confirming that injection of the contrast agent enhanced the image of the brain glioblastoma area.

3. Based on PSNR evaluation, the values ranged from 13.77–20.09 dB.

In conclusion, in this study, the MNP-PDPN contrast agent was useful for early detection of brain glioblastoma. Future research to develop a theragnostic technology for simultaneous diagnosis and treatment of glioblastoma using MNPs-PDPN is needed.

[References]

[1] Mbih Jerome Tosam, “The Role of Philosophy in Modern Medicine”, Open Journal of Philosophy, Vol. 4, No. 1, PP. 75-84 (2014)

[2] Rui Chen, Michael Snyder, “Promise of personalized omics to precision medicine”, WIREs Mechanisms of Disease, Vol. 5, Issue 1, PP. 73-82.(2013)

[3] R. Li, X. Chen, Y. You, X. Wang, Y. Liu, Q. Hu, W. Yan, “Comprehensive portrait of recurrent glioblastoma multiforme in molecular and clinical characteristics”, Oncotarget. 6(31), 30968 (2015).

[4] L. B. Nilsen, A. Fangberget, O. M. Geier, O.

Engebraaten, E. Borgen, D. R. Olsen, T. Seierstad, "Associations Between Tumor Vascularization Assessed by In Vivo DCE-MRI and the Presence of Disseminated Tumor Cells in Bone Marrow in Breast Cancer Patients at the Time of Diagnosis", J. Magn. Reson. Imaging 40(6), 1382 (2014).

[5] Y. Zhang, B. Zhang, F. Liu, J. Luo, J. Bai, "In vivo tomographic imaging with fluorescence and MRI using tumor-targeted dual-labeled nanoparticles", Int. J. Nanomedicine 9, 33 (2014).

[6] Kato Y, Kaneko MK, Kunita A, Ito H, Kameyama A, Ogasawara S, Matsuura N, Hasegawa Y, Suzuki-Inoue K, Inoue O, Ozaki Y, Narimatsu H., " Molecular analysis of the pathophysiological binding of the platelet aggregation-inducing factor podoplanin to the C-type lectin-like receptor CLEC-2", Cancer Sci. 99, 54–61(2008)

[7] Jinhao G, Hongwei G and Bing Xu, "Multifunctional Magnetic Nanoparticles: Design, Synthesis, and Biomedical Applications" Accounts of Chemical Research, 42(8) PP. 1097–107(2009)

[8] *Hazra S and Ghosh N N, "Preparation of nanoferrites and their applications", J. Nanosci. Nanotechnol., 14(2), PP. 1983–2000(2014)*

[9] *Ito A, Shinkai M, Honda H and Kobayashi, " Medical application of functionalized magnetic nanoparticles", J. Biosci. Bioeng. 100(1), PP. 1–11(2005)*

[10] *Pu Y, Tao X, Zeng X, Le Y and Chen, "Synthesis of Co–Cu–Zn doped Fe3O4 nanoparticles with tunable morphology and magnetic properties", J. Magn. Magn. Mater., 322(14) pp. 1985–1990(2010)*

[11] *Lee J H, Jang J T, Choi J S, Moon S H, Noh S H, Kim J W et al., "Exchange-coupled magnetic nanoparticles for efficient heat induction", Nat. Nanotechnol. 6, pp. 418–22(2011)*

[12] *Lu J, Ma S, Sun J, Xia C, Liu C, Wang Z et al., "Manganese ferrite nanoparticle micellar nanocomposites as MRI contrast agent for liver imaging", Biomaterials, 30(15), PP. 2919–28 (2009)*

[13] *Baaziz W, Pichon B P, Liu Y, Grenèche J M, Ulhaq-Bouillet C, Terrier E et al., "Tuning of synthesis conditions by thermal decomposition toward core–shell CoxFe1−xO@CoyFe3−yO4 and CoFe2O4 nanoparticles with spherical and cubic shapes", Chem. Mater., 26(17), PP. 5063–5073(2014)*

[14] S. Rajkumar, G. Malathi, "A Comparative Analysis on Image Quality Assessment for Real Time Satellite Images", Indian Journal of Science and Technology, Vol. 9, No. 34, PP. 1-11(2016)